

Supporting Information

Confined Replacement Synthesis of SnSe Nanoplates in N-Doped Hollow Carbon Nanocages for High-Performance Sodium-Ion Batteries

Xiang Hu,^b Xuhui Yang,^d Yangjie Liu,^{b,c} Min Qiu,^b Zhidong Tian,^b Yao Guo,^b Jun Yuan,^{b,c} Yichun Ding,^{a,b} Hongbing Zhan,^{*a,c} Zhenhai Wen^{*a,b}

a. Fujian Science & Technology Innovation Laboratory for Optoelectronic Information of China, Fuzhou, Fujian 350108, China.

b. CAS Key Laboratory of Design and Assembly of Functional Nanostructures, and Fujian Provincial Key Laboratory of Nanomaterials, Fujian Institute of Research on the Structure of Matter, Chinese Academy of Sciences, Fuzhou, Fujian 350002, China.

c. College of Materials Science and Engineering, Fuzhou University, Fuzhou, Fujian 350108, China

d. College of Environmental and Resource Sciences, Fujian Normal University, Fuzhou, Fujian 350007, China

*Corresponding author.

Email address: hbzhan@fzu.edu.cn, wen@fjirsm.ac.cn

Experimental Section

Synthesis of ZIF-8 polyhedrons: In a typical synthesis, 3 g of $\text{Zn}(\text{CH}_3\text{COO})_2 \cdot 2\text{H}_2\text{O}$ was dissolved in 50 mL of deionized water. Then this solution was rapidly injected into 50 mL of an aqueous solution containing 9.11 mg of cetyltrimethylammonium bromide (CTAB) and 11.165 g of 2-Methylimidazole. Subsequently, the mixed solution was stirred for 15 min and aged for 3 h at room temperature. Finally, the white powder was collected by centrifugation, washed with deionized water and ethanol several times.

Synthesis of ZnSe@NC: 100 mg ZIF-8 polyhedrons were dispersed in 100 mL tris(hydroxymethyl)methyl aminomethane (Tris-buffer solution, 10 mM) by sonication for 20 min. After that, 50 mg of dopamine hydrochloride (PDA) was added under continuous magnetic stirring for 3 h. The resulting ZIF-8@PDA polyhedrons were harvested by centrifugation, washed with deionized water and ethanol for several times, and dried at 60 °C overnight. To attain the ZnSe@NC, the as-prepared ZIF-8@PDA polyhedrons and selenium powder were mixed by grinding with a mass ratio of 1:2, and firstly pyrolyzed at 300 °C for 2 h with a heating rate 2 °C min⁻¹, then the temperature was further increased to 500 °C with the same heating rate and maintained for 1 h under Ar/H₂ (5%) atmosphere.

Synthesis of SnSe@N-HCNs: The ZnSe@NC polyhedrons (100 mg) were dispersed in 60 mL of deionized water with sonication for 30 min. Then, 2 mmol of stannous acetate ($\text{C}_4\text{H}_6\text{O}_4\text{Sn}$) was added to the above solution and stirring for 30 min. The mixture dispersion was transferred into 100 mL Teflon-lined stainless-steel autoclave and heated at 150 °C for 10 h. Finally, the yolk-shell structured SnSe@N-HCNs nanocomposite was collected by centrifugation and dried at 60 °C under vacuum.

Synthesis of SnSe@NC: For comparison, the SnSe@NC were prepared through hydrothermal method. Typically, 50 mg of PDA and 2 mmol of $\text{C}_4\text{H}_6\text{O}_4\text{Sn}$ was dissolved in 60 mL of distilled water, while 2 mmol selenium powder was dissolved in 10 ml of hydrazine hydrate. Then, the two solutions were mixed with violent stirring for 30 min. The mixed

solution was transferred into 100 mL Teflon-lined stainless-steel autoclave and heated at 150 °C for 10 h. After cooled to room temperature naturally, the black product was collected by centrifugation. To enhance the crystallinity of SnSe@NC composites, the final product was annealed at 500 °C for 2 h with a heating rate of 2 °C·min⁻¹ under Ar/H₂ (5%) atmosphere.

Synthesis of Na₃V₂(PO₄)₃/C cathode: The Na₃V₂(PO₄)₃/C hollow microspheres was prepared by via a simple hydrothermal treatment and subsequent calcination method. Firstly, 0.5M oxalic acid was dissolved in 30 mL of deionized water containing 0.02 M of glucose and 0.2 mmol of CTAB at 80 °C under vigorous stirring. Subsequently, V₂O₅, NH₄HPO₄ and NaOH in a molar ratio of 1:3:3 was successively dissolved into the aforementioned solution under vigorous stirring. Afterward, 50 mL isopropanol was added dropwise to the solution and further stirred for 30 min. The consequent suspension was then transferred to a 100 mL Teflon-lined stainless-steel autoclave and maintained at 180 °C for 24 h. After cooling to room temperature, the product was obtained by centrifugation and followed by a freeze-drying process. Finally, the Na₃V₂(PO₄)₃/C hollow microspheres was obtained by annealing at 750 °C for 6 h under Ar/H₂ (5%) atmosphere.

Characterizations: The field emission scanning electron microscopy (FESEM, Hitachi SU-8020), transmission electron microscopy (TEM, Tecnai F20), XRD patterns (Miniflex600) and Raman spectra (Raman Microscope, 532) were performed to characterize the morphology, structure and chemical components of the samples. Thermogravimetric analysis (TGA) was conducted on NETZSCH STA449F3 instrument. X-ray photoelectron spectroscopy (XPS) was performed on ESCALAB 250. Nitrogen adsorption-desorption measurements were tested at 77 K with an automated gas sorption analyzer (Hiden IGA100B).

Electrochemical Characterizations: The 2032 typed coin cells were assembled in an an argon-filled glove box (< 0.01 ppm of moisture and oxygen contents). For the half-cell, the working electrode was prepared by casting a slurry of active materials, acetylene black, and sodium carboxymethyl cellulose with a weight ratio of 8:1:1 onto a copper foil and drying under

vacuum at 100 °C for overnight. The average mass loading of the active material was controlled to be approximately 1.2-1.5 mg cm⁻². The homemade sodium metal foil was used as the counter and reference electrode. Glass fiber filter paper (GF/D, Whatman) was used as the separator. 1 M NaClO₄ dissolved in the mixture of ethylene carbonate (EC)/propylene carbonate (PC) (1:1 by volume) with 5 wt.% fluoroethylene carbonate (FEC) was used as the electrolyte. In the case of the Na₃V₂(PO₄)₃/C//SnSe@N-HCNs sodium-ion full cell, the cathode was prepared by casting a slurry of Na₃V₂(PO₄)₃/C hollow microspheres, carbon black and binder (LA-132) with a weight ratio of 8:1:1 onto an aluminum foil and drying under vacuum at 100 °C for overnight. To avoid the loss of limited Na⁺ ions in the full cell, the SnSe@N-HCNs anode is electrochemically pre-sodiated for five cycles in half cell to form a stable SEI layer. The galvanostatic charging/discharging (GCD) tests were carried out on a LAND multichannel battery test system (Wuhan Kingnuo Electronic Co., China) at room temperature. The galvanostatic intermittent titration technique (GITT) tests were measured under constant-current conditions at 0.2 A g⁻¹ for 20 min and rest intervals for 2 h after the 10th cycles. Cyclic voltammetry (CV) curves were tested on a CHI660E electrochemical workstation and electrochemical impedance spectroscopy (EIS) over a frequency range from 0.01 Hz to 100 kHz.

Calculation Method: DFT calculations were performed with periodic super-cells under the generalized gradient approximation (GGA) using the Perdew-Burke-Ernzerhof (PBE) function for exchange-correlation and the ultrasoft pseudopotentials for nuclei and core electrons. The Kohn-Sham orbitals were expanded in a plane-wave basis set with a kinetic energy cutoff of 30 Ry and the charge-density cutoff of 300 Ry. The energy ΔE can be calculated by the following equation:

$$\Delta E = E_{\text{tot}} - E_{\text{str1}} - E_{\text{str2}}$$

where E_{tot} is the total energy of compound obtained from DFT calculations, E_{str} is the energy of each structure. The Brillouin-zones were sampled with a k-point with Gamma point. A supercell of $3 \times 3 \times 1$ is adopted, with a vacuum layer of $\sim 15 \text{ \AA}$ to remove the slab interaction in the z direction. All the DFT calculations are implemented by the PW modules contained in the Quantum ESPRESSO distribution.

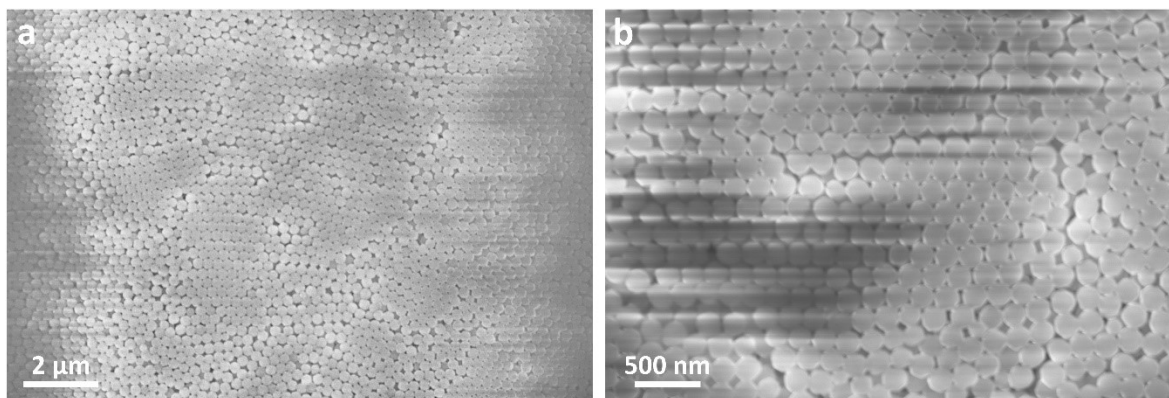


Figure S1. (a, b) SEM images of ZIF8.

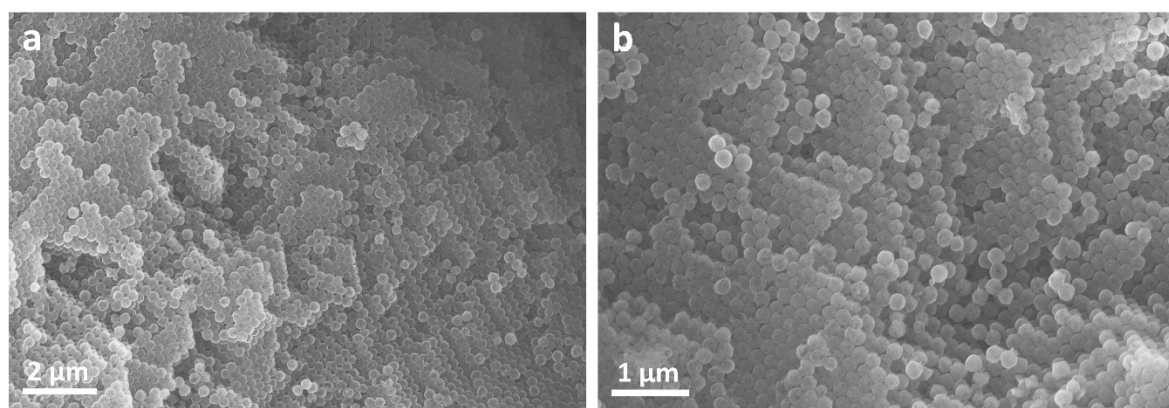


Figure S2. (a, b) SEM images of ZIF8@NC.

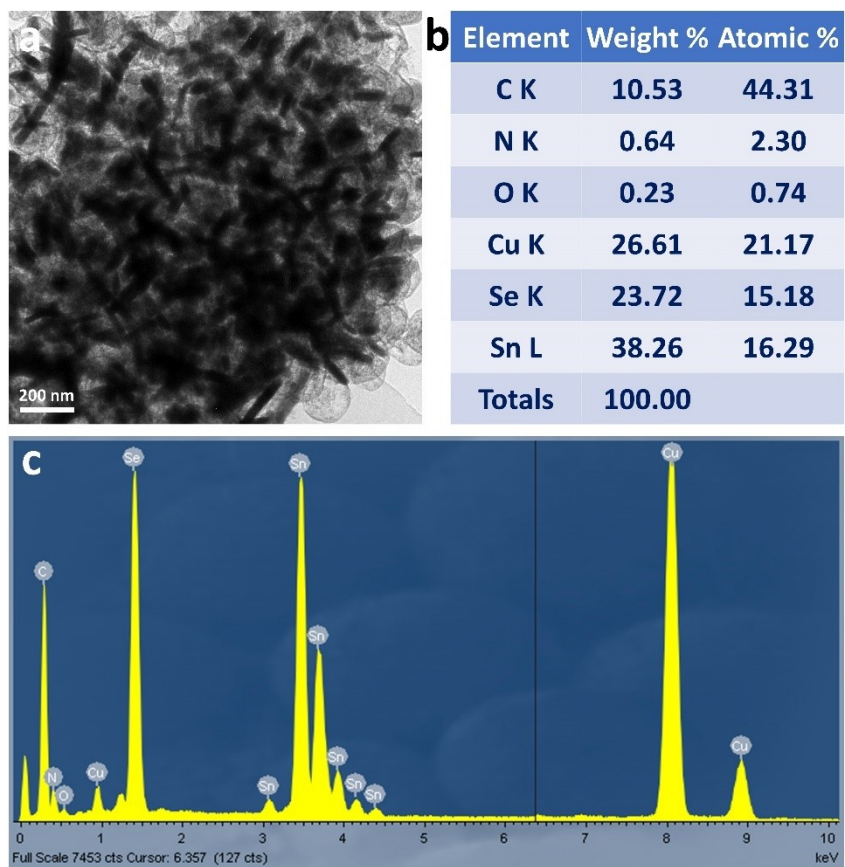


Figure S3. (a) TEM image, (b, c) the corresponding EDX spectrum and the element content of SnSe@N-HCNs.

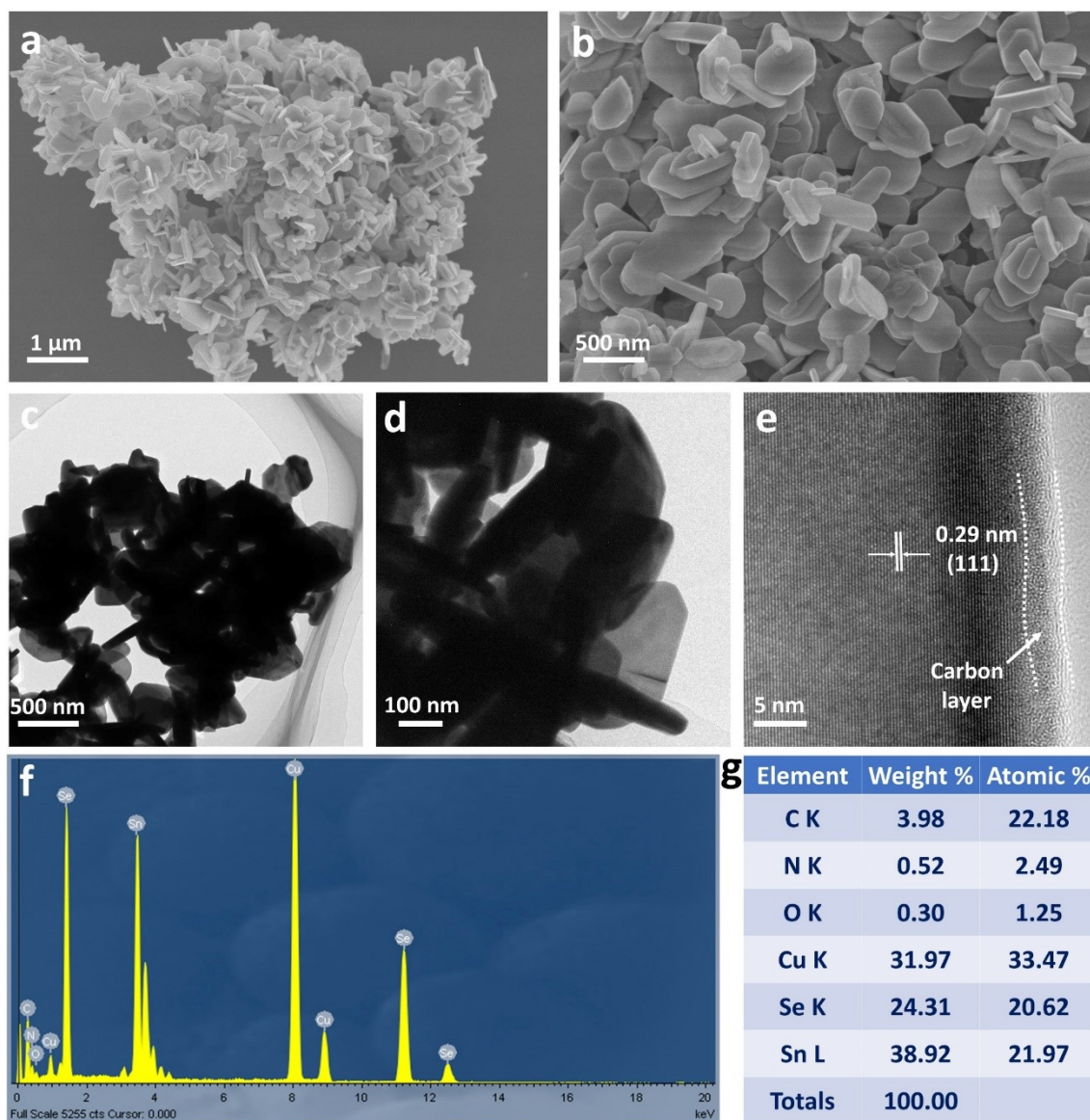


Figure S4. (a, b) SEM images, (c, d) TEM, (e) HRTEM images, (f) the corresponding EDX spectrum and (g) the element content conta of SnSe@NC nanoplates. The results indicate that the N atoms have been successfully doped into the carbon matrix.

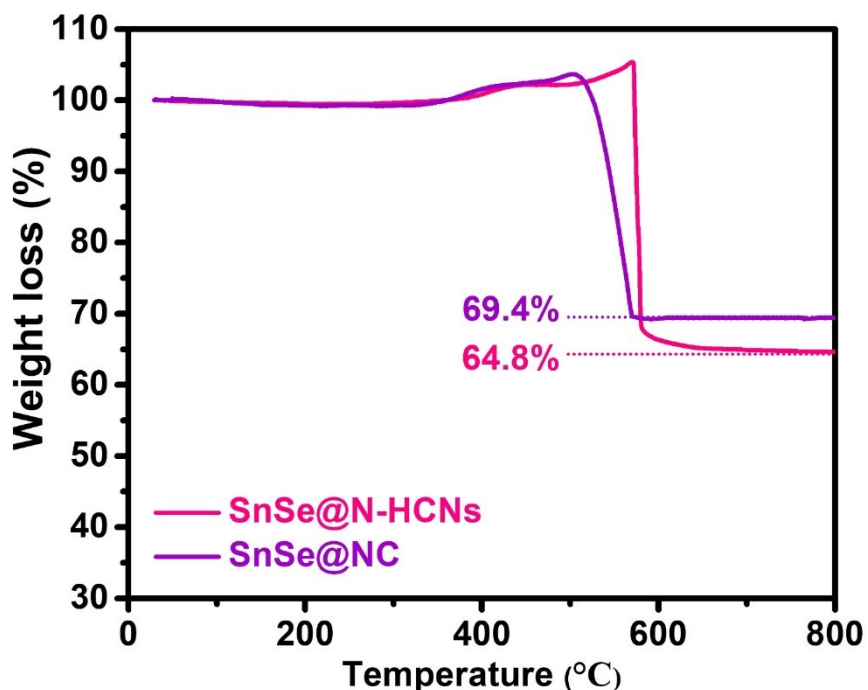
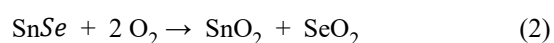


Figure S5. TGA curves of SnSe@N-HCNs and SnSe@NC in an air with a heating rate of 10 °C min⁻¹.

TGA analysis:

From the TGA curves, the weight increase in the range from 400 to 570 °C of SnSe@N-HCNs composite can be attributed to the oxidation of SnSe into SnO₂. And the following weight loss can be ascribed to the carbon burn out. The total reaction can be simply written as:



Therefore, the SnSe@N-HCNs composite can be calculated according to the following equation:

$$\text{SnSe (wt\%)} = \frac{\text{molecular weight of SnSe}}{\text{molecular weight of SnO}_2} \times \frac{\text{final weight of SnO}_2}{\text{initial weight of SnSe@N-HCNs}} \times 100\%$$

Based on the final residual weight of the SnO₂, the content of carbon in SnSe@N-HCNs and SnSe@NC composite is calculated as about 15% and 9%, respectively.

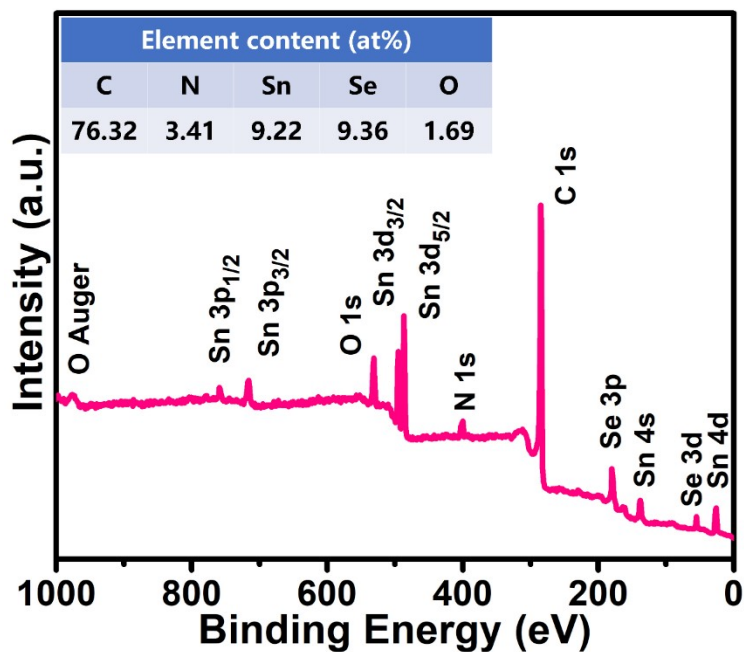


Figure S6. The survey XPS spectrum of SnSe@N-HCNs (the inset shows the element content). The result show that the atomic percentage ratio of Sn and Se is calculated to be about 1:1.04, an ideal chemical stoichiometry of SnSe.

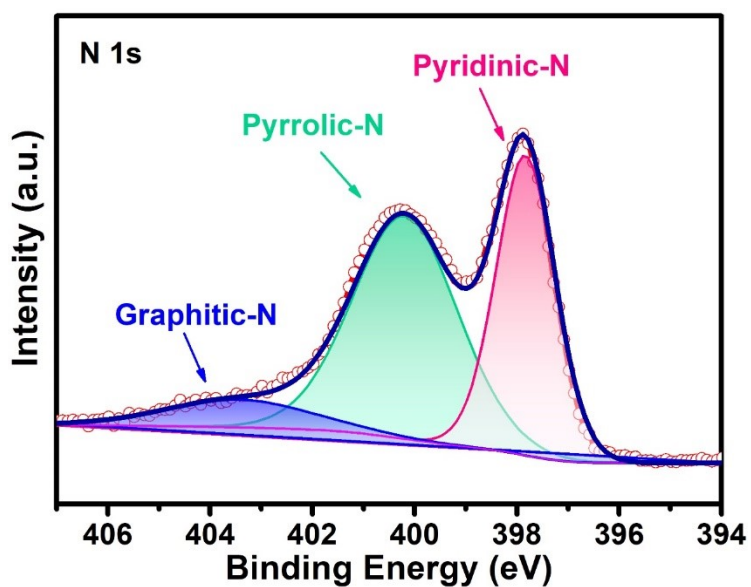


Figure S7. The high-resolution XPS spectra of N 1s for the SnSe@N-HCNs.

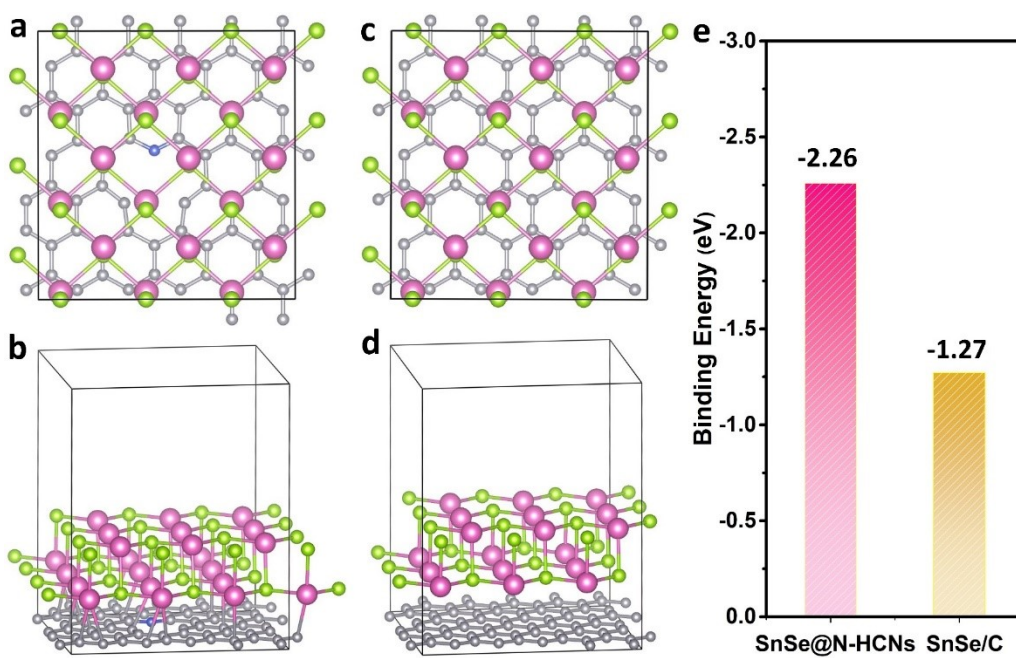


Figure S8. Top and side view of the optimized structure of (a, b) SnSe@N-HCNs and (c, d) SnSe@C. (e) The calculated binding energy of SnSe@N-HCNs and SnSe@C.

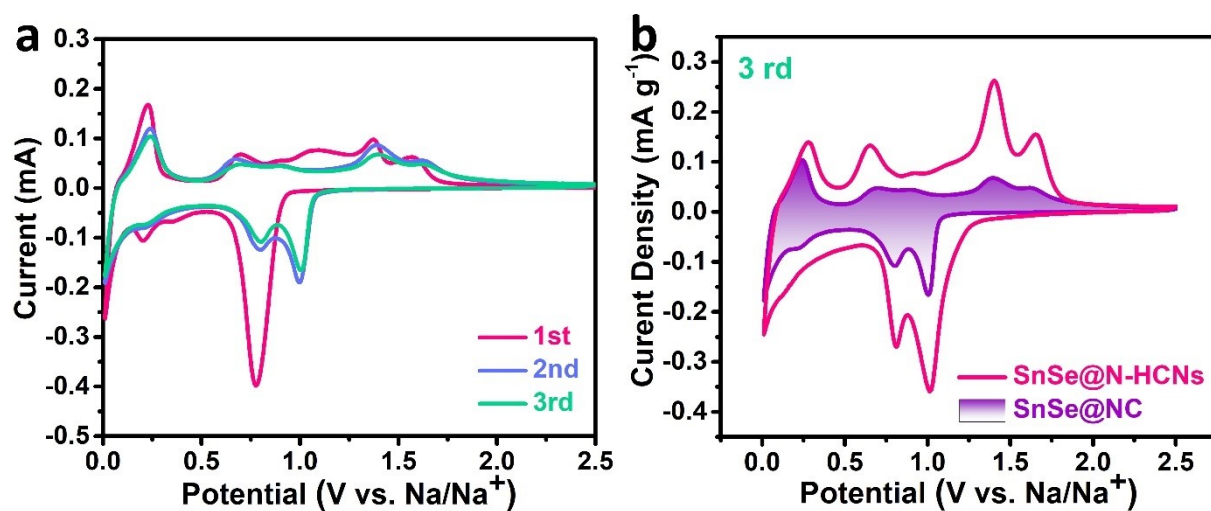


Figure S9. CV curves of the (a) SnSe@NC and (b) CV curves of the SnSe@N-HCNs and SnSe@NC for the 3rd cycle at a scan rate of 0.1 mV s⁻¹.

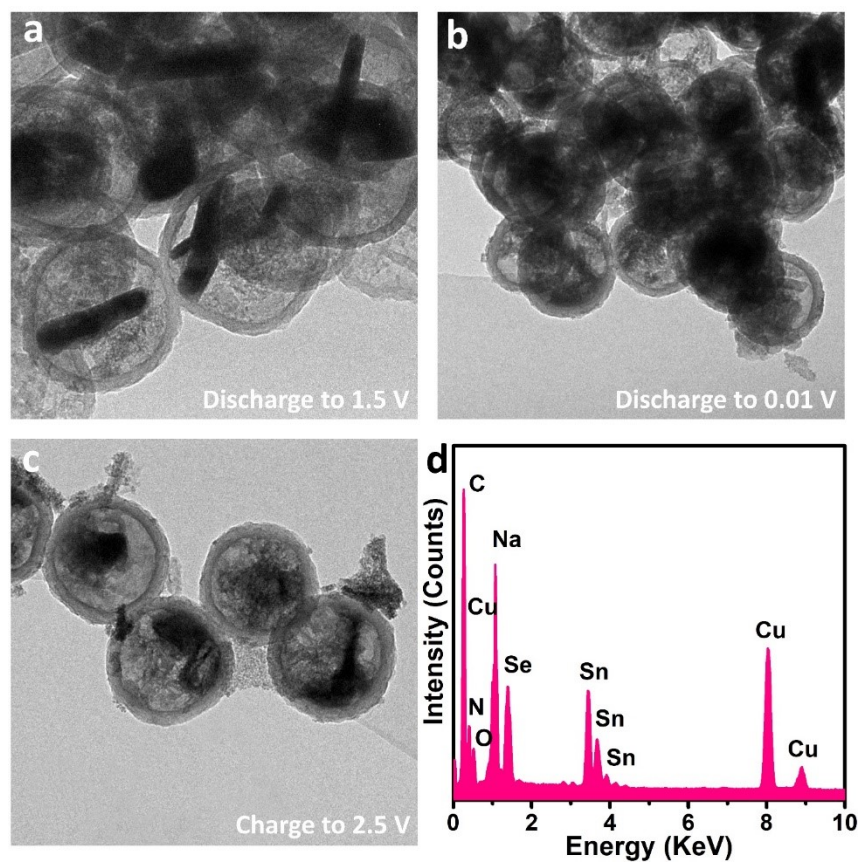


Figure S10. Ex situ TEM images of SnSe@N-HCNs electrode at various potentials during initial cycle: discharge states of (a) 1.5 V and (b) 0.01 V, (c) charge state of 2.5 V and (d) the corresponding EDX spectrum.

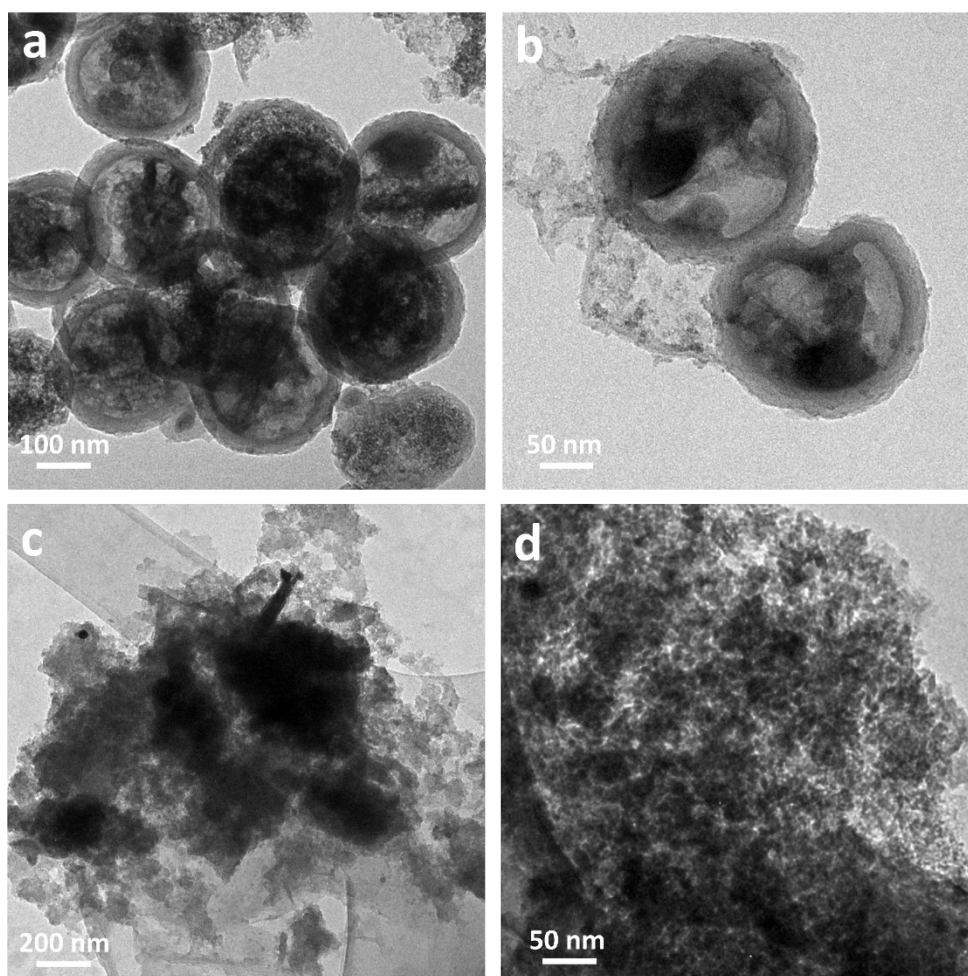


Figure S11. TEM images of the (a, b) SnSe@N-HCNs and (c, d) SnSe@NC electrode after 200 cycles at 0.2 A g^{-1} .

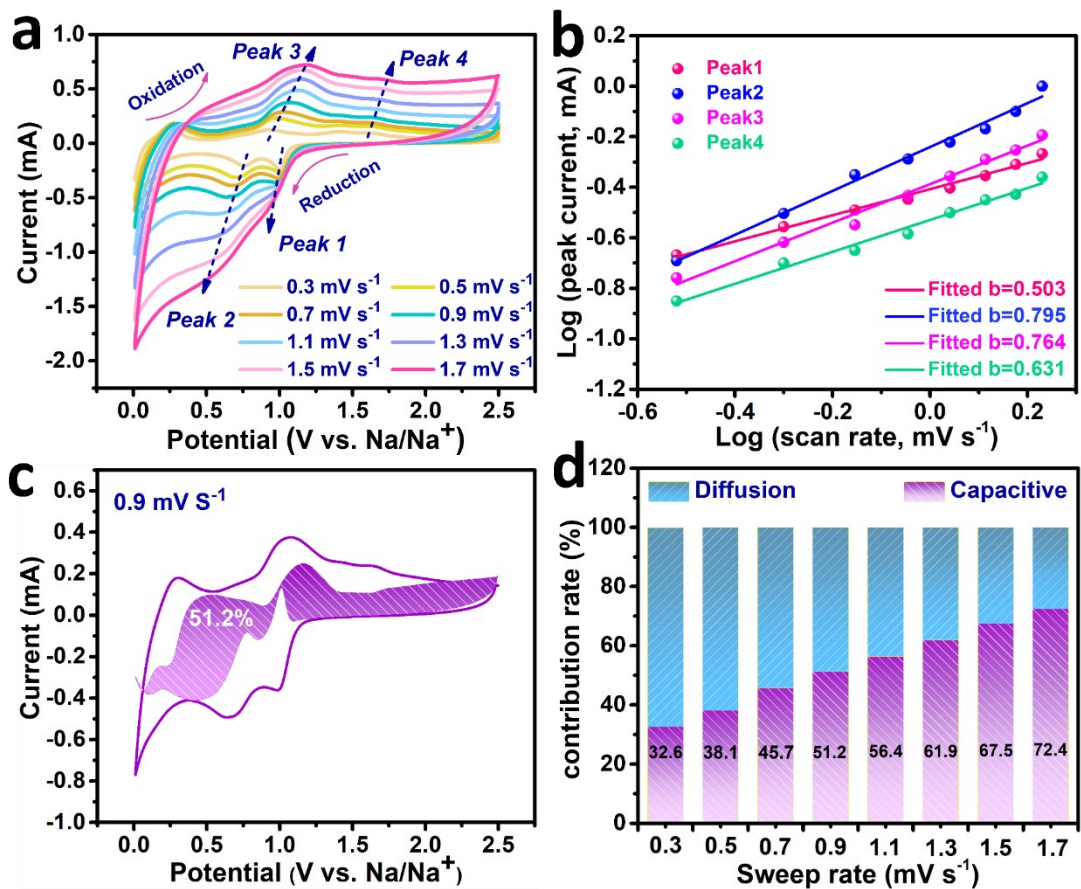


Figure S12. Dynamics analysis: (a) CV curves at various scan rates from 0.3 to 1.7 mV s⁻¹, (b) linear relationships between logarithm currents and logarithm sweep rate, (c) capacitive contribution at 0.9 mV s⁻¹, (d) calculated capacitive contributions at different sweep rate for the SnSe@NC.

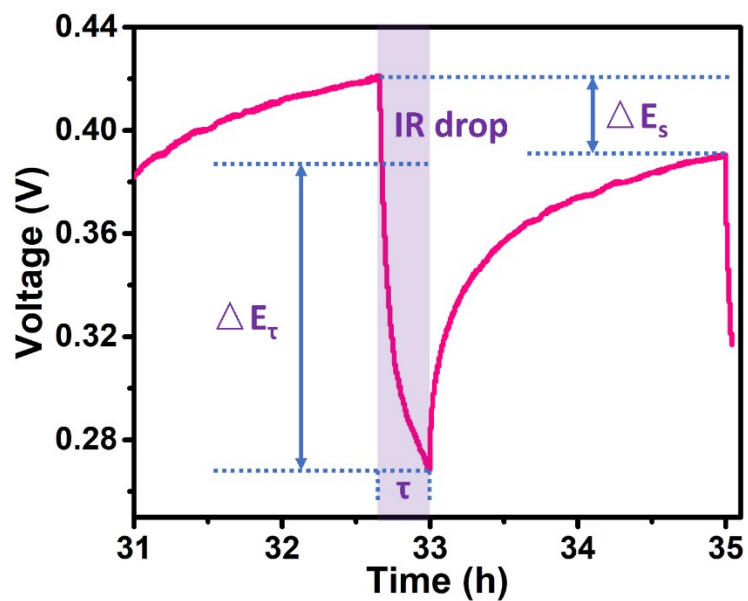


Figure S13. The local GITT curve. The determination of ΔE_τ (the change of voltage during the current pulse) and ΔE_s (the quasi-thermodynamic equilibrium potential difference between before and after the current pulse) from the measured GITT profiles.

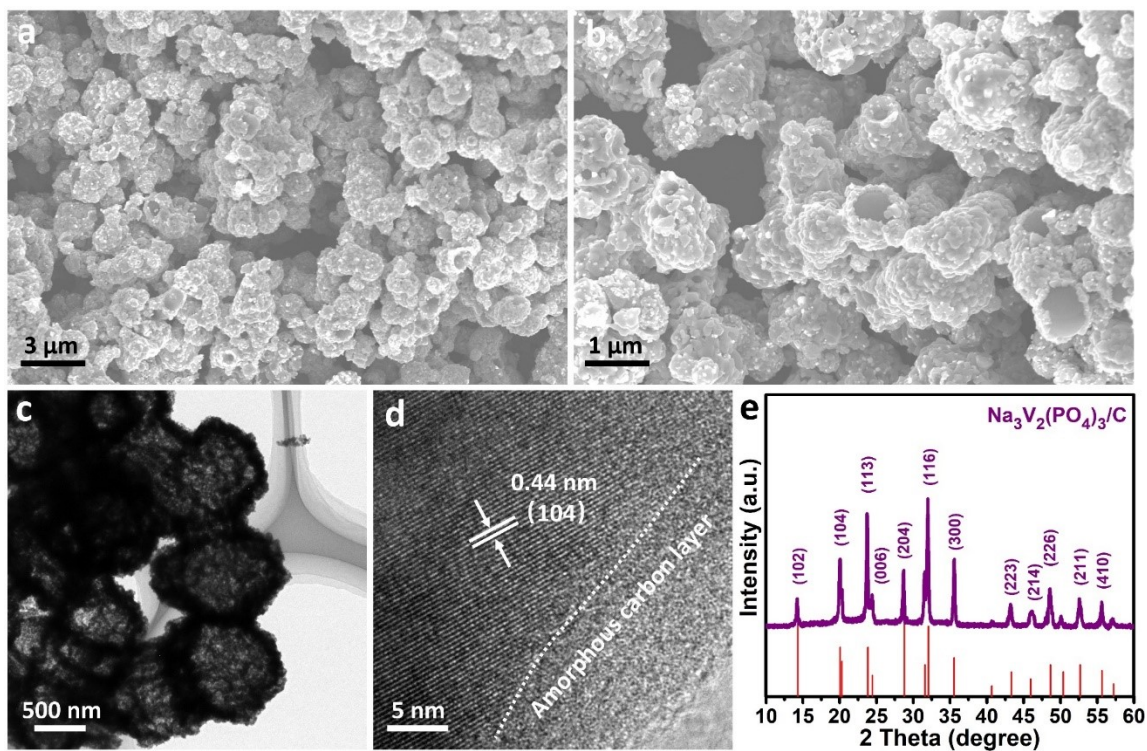


Figure S14. (a, b) SEM images, (c) TEM, (d) HRTEM and (e) XRD pattern of the $\text{Na}_3\text{V}_2(\text{PO}_4)_3/\text{C}$.

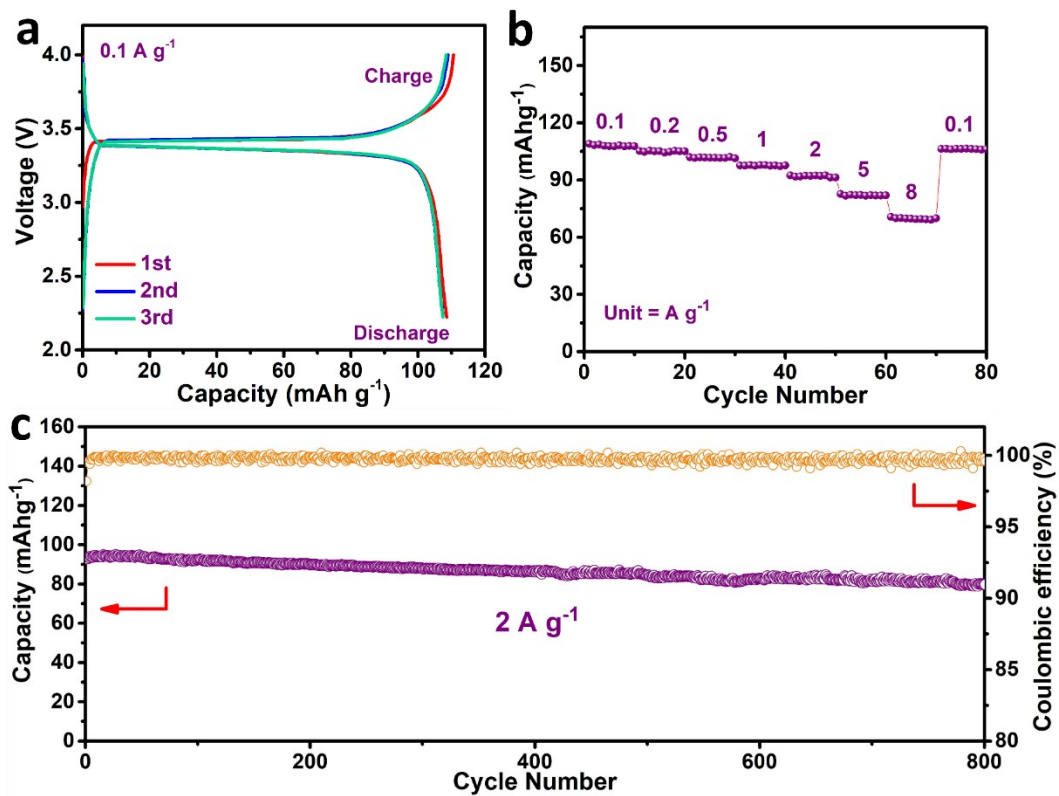


Figure S15. (a) representative discharge-charge curves at 0.1 A g^{-1} at a potential range of 2.2–4.0 V, (b) Rate capability and (c) long cycling performance at 2 A g^{-1} of the $\text{Na}_3\text{V}_2(\text{PO}_4)_3/\text{C}$.

Table S1. The electrochemical performances comparison of SnSe@N-HCNs and previously reported Tin-based compound anode for SIBs.

Materials	Voltage range(V)	Current density (mA g ⁻¹)	Cycle number	Specific capacity (mAh g ⁻¹)	Reference
SnSe@N-HCNs	0.01-2.5	200	200	516	This work
		1000	1000	425	
SnSe@NSC	0.01-3.0	1000	500	302.6	Ref 1
SnSe@C	0.01-3.0	1000	500	283.8	Ref 2
SnSe/CNF	0.01-2.5	1000	500	405	Ref 3
a-SnSe/rGO	0.01-3.0	1000	1400	398	Ref 4
NG@SnSe/C	0.01-2.5	500	100	405.4	Ref 5
SnSe NSCs	0.01-3.0	200	100	271	Ref 6
SnSe NPs	0.01-3.0	1000	300	328.4	Ref 7
SnS/SnO _x	0.01-2.0	300	600	247	Ref 8
SnS/C NFs-650 °C	0.01-2.5	200	500	349	Ref 9
SnS ₂ /NS-CNT	0.01-2.5	200	80	417	Ref 10
SnSe ₂ NCs/C	0.01-3.0	1000	1000	363	Ref 11
SnSSe/C	0.01-3.0		500	400.5	Ref 12
		1000			
SnSe _{0.5} S _{0.5} /C	0.01-3.0	200	100	430	Ref 13
Ti _{0.25} Sn _{0.75} S ₂	0.01-2.5	400	1000	307	Ref 14
SnS@C	0.01-3.0	100	200	440.3	Ref 15

Supplementary References

- [1] J. Hou, Z. Zhu, C. Li, J. Zhang, S. Shen, Z. Yao, T. Liu, W. Li, X. Xia, Y. Yang, Spatially confined synthesis of SnSe spheres encapsulated in N, Se dual-doped carbon networks toward fast and durable sodium storage, *ACS Appl. Mater Interfaces*, **2022**, 14, 4230.
- [2] F. Kong, Z. Han, S. Tao, B. Qian, Core-shell structured SnSe@C microrod for Na-ion battery anode, *J. Energy Chem.*, **2021**, 55, 256.
- [3] J. Xia, Y. Yuan, H. Yan, J. Liu, Y. Zhang, L. Liu, S. Zhang, W. Li, X. Yang, H. Shu, X. Wang, G. Cao, Electrospun SnSe/C nanofibers as binder-free anode for lithium-ion and sodium-ion batteries, *J. Power Sources*, **2020**, 449, 227559.
- [4] M. Wang, A. Peng, H. Xu, Z. Yang, L. Zhang, J. Zhang, H. Yang, J. Chen, Y. Huang, X. Li, Amorphous SnSe quantum dots anchoring on graphene as high performance anodes for battery/capacitor sodium ion storage, *J. Power Sources*, **2020**, 469, 228414.
- [5] C. Lu, Z. Z. Li, Z. Xia, H. N. Ci, J. S. Cai, Y. Z. Song, L. H. Yu, W. J. Yin, S. X. Dou, J. Y. Sun, Z. F. Liu, Confining MOF-derived SnSe nanoplatelets in nitrogen-doped graphene cages via direct CVD for durable sodium ion storage, *Nano Res.*, **2019**, 12, 3051.
- [6] S. Yuan, Y. H. Zhu, W. Li, S. Wang, D. Xu, L. Li, Y. Zhang, X. B. Zhang, Surfactant-free aqueous synthesis of pure single-crystalline SnSe nanosheet clusters as anode for high energy-and power-density sodium-ion batteries, *Adv. Mater.*, **2017**, 29, 1602469.
- [7] W. Wang, P. Li, H. Zheng, Q. Liu, F. Lv, J. Wu, H. Wang, S. Guo, Ultrathin layered SnSe nanoplates for low voltage, high-rate, and long-life alkali-ion batteries, *Small*, **2017**, 13, 1702228.
- [8] H. Bian, Z. Li, X. Xiao, P. Schmuki, J. Lu, Y. Y. Li, Anodic synthesis of hierarchical SnS/SnO_x hollow nanospheres and their application for high-performance Na-ion batteries, *Adv. Funct. Mater.*, **2019**, 29, 1901000.
- [9] J. Xia, L. Liu, S. Jamil, J. Xie, H. Yan, Y. Yuan, Y. Zhang, S. Nie, J. Pan, X. Wang, G. Cao, Free-standing SnS/C nanofiber anodes for ultralong cycle-life lithium-ion batteries and sodium-ion batteries, *Energy Storage Mater.*, **2019**, 17, 1.
- [10] Z. Liu, A. Daali, G. L. Xu, M. Zhuang, X. Zuo, C. J. Sun, Y. Liu, Y. Cai, M. D. Hossain, H. Liu, K. Amine, Z. Luo, Highly reversible sodiation/desodiation from a carbon-sandwiched SnS₂ nanosheet anode for sodium ion batteries, *Nano Lett.*, **2020**, 20, 3844.

- [11] H. Chen, Z. Mu, Y. Li, Z. Xia, Y. Yang, F. Lv, J. Zhou, Y. Chao, J. Wang, N. Wang, S. Guo, SnSe₂ nanocrystals coupled with hierarchical porous carbon microspheres for long-life sodium ion battery anode, *Sci. China Mater.*, **2019**, 63, 483.
- [12] L. Cao, S. Fang, B. Xu, B. Zhang, C. Wang, Z. Xiao, G. Zou, H. Hou, X. Ou, X. Ji, Enabling reversible reaction by uniform distribution of heterogeneous intermediates on defect-rich SnSSe/C layered heterostructure for ultralong-cycling sodium storage, *Small*, **2022**, 18, 2202134.
- [13] Q. Tang, Y. Cui, J. Wu, D. Qu, A. P. Baker, Y. Ma, X. Song, Y. Liu, Ternary tin selenium sulfide (SnSe_{0.5}S_{0.5}) nano alloy as the high-performance anode for lithium-ion and sodium-ion batteries, *Nano Energy*, **2017**, 41, 377.
- [14] Y. Huang, M. Xie, Z. Wang, Y. Jiang, G. Xiao, S. Li, L. Li, F. Wu, R. Chen, Fast sodium storage kinetics of lantern-like Ti_{0.25}Sn_{0.75}S₂ connected via carbon nanotubes, *Energy Storage Mater.*, **2018**, 11, 100.
- [15] P. He, Y. Fang, X. Y. Yu, X. W. D. Lou, Hierarchical nanotubes constructed by carbon-coated ultrathin SnS nanosheets for fast capacitive sodium storage, *Angew. Chem. Int. Ed.*, **2017**, 56, 12202.